High-Efficiency PbS Quantum-Dot Solar Cells with Greatly Simplified Fabrication Processing via "Solvent-Curing"

Lu, Kunyuan; Wang, Yongjie; Liu, Zeke; Han, Lu; Shi, Guozheng; Fang, Honghua; Chen, Jun; Ye, Xingchen; Chen, Si; Yang, Fan

Published in:
Advanced materials

DOI:
10.1002/adma.201707572

Publication date:
2018

WILEY-VCH

DOI: 10.1002/((please add manuscript number))
Article type: Communication

High-Efficiency PbS Quantum Dots Solar Cells with Greatly Simplified Fabrication Processing via "Solvent-Curing"

Kunyuan Lu,‡ Yongjie Wang,‡ Zeke Liu, Lu Han, Guozheng Shi, Honghua Fang, Jun Chen, Xingchen Ye, Si Chen, Fan Yang, Artem G. Shulga, Tian Wu, Mengfan Gu, Sijie Zhou, Jian Fan, Maria Antonietta Loi and Wanli Ma**

K. Lu, Y. Wang, Z. Liu, L. Han, G. Shi, S. Chen, F. Yang, T. Wu, M. Gu, S. Zhou, Prof. J. Fan, and Prof. W. Ma*
Jiangsu Key Laboratory for Carbon-Based Functional Materials & Devices, Institute of Functional Nano & Soft Materials (FUNSOM), Soochow University, 199 Ren-Ai Road, Suzhou Industrial Park, Suzhou, 215123 Jiangsu, P. R. China.
E-mail: wlma@suda.edu.cn

H. Fang, A. G. Shulga, Prof. M. A. Loi*
Zernike Institute for Advanced Materials University of Groningen, Nijenborgh 4, 9747 AG, The Netherlands.
E-mail: m.a.loi@rug.nl

J. Chen, Prof. X. Ye
Department of Chemistry, Indiana University, Bloomington, 800 E. Kirkwood Ave. Bloomington, IN 47405, United States.

‡ K. Lu and Y. Wang contributed equally to this work.

Keywords: Solar Cells, PbS Quantum Dots, Rinsing Solvent, Solvent-Curing

Abstract:

PbS quantum dots (QDs) solar cells are promising candidates for low-cost solution-processed photovoltaics. However, the device fabrication usually requires 10 more times film deposition and rinsing steps, which is not ideal for scalable manufacturing. In this work, a greatly simplified deposition processing was demonstrated by replacing methanol with acetonitrile (ACN) as the rinsing solvent. We discovered that ACN could effectively "cure" the film cracks generated from the volume loss during the solid-state ligand exchange process, which enabled the deposition of thick and dense films with much less deposition steps. Meanwhile, the aprotic nature of ACN can introduce less trap states during the rinsing process. As a result, with only

3 deposition steps for the active layer, a certified 11.21% power conversion efficiency was obtained, which is the highest efficiency ever reported for PbS QDs solar cells employing solid-state ligand exchange process. More importantly, the simple film deposition processing provides an opportunity for the future application of QDs in low-cost printing optoelectronic devices.

Colloidal lead chalcogenides (PbX) quantum dots (QDs) used for optoelectronic devices have received considerable attention owing to their huge bandgap tunability, multiple-exciton generation effect and facile solution-processing.[1-4] Rapid advances in QDs solar cells by device architecture engineering and surface passivation have led to a reported certified power conversion efficiencies (PCE) of 11.3%.[5] Specially, both single-junction and tandem PbS QDs solar cells show outstanding air stability.[6, 7] However, the prerequisite ligand-exchange during QDs device fabrication renders the manufacturing process extremely complex and costly compared to other solution-processed solar cells, which may largely restrict their future application in industry. The typical as-synthesized PbS QDs are capped with oleic acid ligands, which help to passivate the surface and stabilize QDs in organic solution, but also make them insulated from surrounding QDs. An essential step to realize high performance CQDs photovoltaic devices is exchanging these long chain ligands with short ones and simultaneously remaining good surface passivation.[8] Up to now, there are mainly two ligand exchange methods. (1) Solid-state ligand exchange: the PbS QDs solution is deposited on a substrate and then the QDs film is ligand exchanged with short ligands such as thiols,[9, 10] mercaptopropionic acid (MPA)[11, 12] and iodide[6, 13-15] to remove the electrically insulating oleic acid. Then the rinsing solvent is used to wash away the exchanged long ligands as well as the excess short ligands. To ensure complete ligand exchange and achieve smooth and compact films, the thickness of each layer is normally around a few tens nanometer, [6] which then usually requires 10 times layer by layer (LbL) deposition process to get appropriate thickness for efficient light harvesting.[8] The

solid-state ligand exchange approach has been widely used on PbS QDs solar cells for more than 10 years, and resulted in a highest reported PCE of 10.8%.[16] However, the tedious process and high material consumption will certainly increase the manufacturing cost of QDs solar cells, not suitable for the future industrial application. In recent years, another ligand exchange method (2) "Solution-phase ligand exchange" was reported, in which, the ligand exchange process is completed in solution. The resultant PbS QDs inks can be directly deposited and largely simplify the manufacturing process. Nonetheless, the efficiency of PbS QDs solar cells based on this approach has been lower than those based on solid-state ligand-exchange for a long time. Until very recently, Liu *et al.* developed a new solution-exchange procedure and achieved a PCE of 11.3%, exceeding the best device based on solid-state ligand exchange.[5] However, this procedure requires large consumption of the lead precursors (lead(II) iodide and lead(II) bromide) for ligand exchange,[5] which is not ideal for mass industrial manufacture considering the economic and environmental issues. Meanwhile, this procedure is not as efficient in the control of QD energy levels and doping parameters. A simpler and industry-compatible procedure for PbS QDs film deposition is thus urgently required. Unfortunately, so far very few work has been done to simplify the deposition processing. A representative work was reported using aprotic acetonitrile (ACN) as the ligand exchange solvent in traditional MPA ligand based system[17] to replace widely used methanol (MeOH), which has been demonstrated to be offensive to QDs surface and introduce extra trap states.[18-20] As a result, elongated ligand-exchange time and fewer LbL steps (3 steps) were achieved for the active layer deposition compared to the typical 10 steps for the control devices. Although the obtained PCE of 6.81% is much lower than the state-of-the-art PbS QDs solar cells, this work shows the great importance of solvent engineering in simplifying the fabrication processing of PbS QDs solar cells. Unfortunately, the effect of solvent on QD film morphology during ligand-exchange and rinsing has not been realized and the full potential of solvent engineering requires further investigation.

In this work, we demonstrated that less trap states, optimal film morphology and high-performance devices could be achieved by replacing MeOH with ACN as the rinsing solvent during the LbL process of PbS QD solar cells. We discovered that simply replacing MeOH with ACN could largely reduce trap states during ligand exchange process, resulting in improved device performance. Meanwhile, ACN could "cure" the film cracks generated from the volume loss during the solid-state ligand exchange process, which enabled the deposition of thick and dense films with much less LbL steps. As a result, PbS QDs solar cells with a certified PCE of 11.21% was obtained using only 3 deposition steps for the active layer. To the best of our knowledge, this is the highest PCE ever reported for PbS QDs solar cells employing solid-state ligand exchange method. Moreover, a very close PCE of 10.6% could be realized with only 2 deposition steps. Thus, our results provided a facile approach to greatly simplify the fabrication process of efficient PbS QD solar cells, giving an alternative avenue to promote the application of QDs in low-cost printing optoelectronic devices.

The current most efficient PbS QDs solar cell has a device structure of ITO/ZnO/PbS-TBAI (tetrabutylammonium iodide)/PbS-EDT(1,2-ethanedithiol)/Au, with the device schematic diagram and cross-sectional scanning electron microscope (SEM) image shown in **Figure 1**a, b. For our control devices, the PbS QDs in hexane were spin-coated on ITO/ZnO employing the normal 5 steps LbL process, in which TBAI was dissolved in MeOH for ligand exchange and MeOH was also used as the rinsing solvent (see the Experimental Section for details). Note that, as Song *et al*. recently demonstrated,[20] MeOH as the TBAI-exchange solvent can induce undesirable traps on PbS QDs surface. It is thus desired to use ACN as both ligand-exchange and rinsing solvent to avoid the adverse effect of MeOH and further improve the device efficiency. However, as a proton transfer is necessary to release the bound oleate ligand from QDs surface,[18] currently it is unable to replace the protic MeOH with aprotic ACN as the ligand-exchange solvent in the TBAI based system.[21] It has been reported that PbS QDs ligand exchange can not take place in fully aprotic conditions, even up to 10 min exposure to the

solution of TBAI (10 mM) in ACN.[21] We thus only adopted ACN as the rinsing solvent while still using MeOH as the solvent for ligand-exchange. Surprisingly, as shown in Figure 1c, the simple replacement of MeOH with ACN as the rinsing solvent for the PbS-TBAI layers significantly increases the highest PCE from 9.43% to 10.66%, with the average PCE improved from 8.93%±0.19% to 10.40%±0.18%. The devices reproducibility was confirmed by analyzing the PCEs of 24 devices with MeOH or ACN as the rinsing solvent. We noticed that the improvement mainly stems from the increase of open- circuit voltage (V_{OC}) and fill factor (FF), while the short-circuit current density (J_{SC}) is almost the same (**Table 1**). To explore the detailed mechanisms for the device enhancement when using ACN as the rinsing solvent, we first conducted systematical device characterizations. As shown in the dark *J-V* curves (**Figure 2**a), the leakage current for the ACN-rinsed device is greatly suppressed compared to the device rinsed by MeOH, while the two devices exhibit similar output current in the forward direction, indicating higher rectification ratio and thus better diode characteristics for the ACN rinsed device. To get further insight into the charge recombination kinetics, we studied the variation of J_{SC} as a function of the illumination intensity. The light intensity dependence of the J_{SC} can be described as a power law equation: $J_{sc} \propto I^{\alpha}$, where I is the light intensity. Both values of the exponential factor (α) for the device rinsed with MeOH and ACN are found to be close to unity. This result indicates that bimolecular recombination during the charge sweep-out under short-circuit condition is not serious for both devices. In addition, the light intensity dependence of V_{OC} was also studied according to the following relation: $V_{oc} = \frac{nkT}{q}\alpha \ln(I) + c$, where k is the Boltzmann constant, T the temperature, q the elementary charge, and c a fitting parameter collecting all the terms independent of light intensity. The values of diode ideality factor n are determined to be 1.56 and 1.36 for the device rinsed by MeOH and ACN, as shown in Figure 2c. The lower n for device rinsed with ACN suggests reduced trap-assisted charge recombination.[22] Meanwhile, according to the equation $V_{oc} = \frac{nkT}{q} \ln\left(\frac{J_{sc}}{J_0}\right)$, where J_0 is the

device reverse saturation current density. The values of J_0 for ACN-rinsed device is calculated to be 5.93×10^{-7} mA/cm^2 which is much lower than that of the MeOH-rinsed device (6.94×10^{-6} mA/cm^2). Hence, the reduced recombination and smaller reverse saturation current density J_0 may interpret the enhanced V_{OC} of ACN-rinsed device.[23] To confirm the conclusion, the transient photovoltage (TPV) measurements were performed at open-circuit condition with 1-sun light bias, with the results shown in Figure 2d. The apparently slower voltage decay of ACN-rinsed devices (109.5 μs) compared to that of the MeOH-rinsed devices (91.6 μs) indicates fewer sub-bandgap trap-states and less carrier recombination, which is consistent with the aforementioned results. The effect of rinsing solvent on the device carrier transport behavior in the PbS-TBAI films rinsed by MeOH or ACN was also investigated by utilizing field-effect transistor (FET). The transistors consist of pre-patterned Si/SiO_2 substrate as the gate electrode, Au as the source and drain electrodes, and PbS-TBAI film rinsed with ACN or MeOH. From the FET transfer characteristics (**Figure 3**a), both the MeOH-rinsed and ACN-rinsed transistors exhibit ambipolar transport behavior. Whereas, the ACN-rinsed sample shows more n-type properties with an electron mobility of 1.7×10^{-3} cm^2 V^{-1} s^{-1}, which is 10-fold higher than the 1.6×10^{-4} cm^2 V^{-1} s^{-1} for MeOH-rinsed sample. In addition, the n-channel on/off ratio of 10^4 in ACN-rinsed transistors is much higher than the 10^2 in MeOH-rinsed samples, while no significant difference is observed for the p-channel, indicating significantly enhanced electron transport in ACN-rinsed film due to better passivation of traps. The EDT exchanged PbS QDs layer shows apparent p-type transport behavior (Figure S1), enabling the formation of desired junction with TBAI exchanged PbS QDs layer. The doping densities for each layer were also tested by capacitance voltage measurements (Figure S2), which were summarized in Table S1 together with their mobility values.

Since all experimental conditions for this device fabrication are identical except rinsing solvents, we attribute the suppressed carrier recombination to reduced sub-bandgap states in PbS QDs films rinsed with ACN. This speculation was further verified by the

photoluminescence (PL) measurement. Compared to the film rinsed by MeOH, the ACN rinsed PbS-TBAI film shows almost 10 folds increase in PL intensity (Figure 3b) and doubles the PL lifetime in the fast decay region (Figure 3c and Table S2). Furthermore, nearly-identical absorbance and Fourier transform infrared (FTIR) spectra indicate that the change in rinsing solvents for PbS-TBAI films results in negligible effect on the film thickness and surface ligand (Figure S3). To probe the subtle effect of rinsing solvent on QDs surface, X-ray photoelectron spectroscopy (XPS) was performed. As shown in the high-resolution XPS core spectra of O 1s (**Figure 4**a) and C 1s (Figure 4b), the peak at around 532.5 eV in the O 1s spectrum and 286.4 eV in the C 1s spectrum can be assigned to the bonding oxygen and carbon in methoxyl group respectively, [24-26] which are significantly stronger for QDs film rinsed with MeOH than those with ACN. Moreover, an apparent peak at 533.9 eV ascribed to the physically absorbed methanol, can be detected in MeOH-rinsed sample while it is absent in the ACN-rinsed film. [24-26] These results demonstrate that more methoxyl groups and MeOH molecules are attached to PbS QDs surface when the film is rinsed by MeOH, which indicates that some iodides on the QD surface may be replaced by the methoxyl group. As a result, I/Pb ratios in MeOH and ACN rinsed sample are 0.61 and 0.73 respectively (Figure S4). A higher I/Pb ratio indicates a higher-quality surface passivation,[5, 15] resulting in less recombination and higher device performance.

Meanwhile, considering the smaller reverse saturation current density J_0 and lower leakage current for ACN-rinsed device can partly due to film morphology, we speculated that the film quality may be affected by the rinsing solvents, and we conducted morphology investigation using scanning electron microscopy. There usually exist numerous cracks on the ligand-exchang PbS QDs film due to the huge volume loss, as shown in Figure S5a.[27] However, we found that an almost crack-free surface morphology appeared when ACN was used to rinse PbS-TBAI film instead of MeOH (Figure S5b). To further verify the film curing function of ACN, we performed the ligand-exchange and rinsing process on a thicker PbS QDs film (~70 nm compared to the conventional ~35 nm), since a thicker layer exhibits more cracks and is

harder to recover. As shown in Figure 4c, large cracks exist in the PbS-TBAI film rinsed by MeOH while the ACN-rinsed film shows surprisingly crack-free surface morphology even for such a thick film (Figure 4d). Furthermore, to probe the curing effect in a real device, we conducted the cross-sectional SEM for the samples sectioned by focused ion beam (FIB) with an intact structure of ITO/ZnO/PbS (80mg/mL)-TBAI×3/PbS-EDT×2/Au. The PbS-TBAI layers were rinsed by MeOH and ACN respectively. As shown in Figure 4e, apparently some cracks locate within the MeOH rinsed active layer crossing the whole PbS-TBAI film. Additionally, these film voids are not fully filled by QDs during the deposition of the subsequent PbS-EDT layer, which may result in reduced film quality and diode properties. However, the ACN-rinsed device shows pinhole-free film (Figure 4f), which corresponds well with the SEM top-view morphology, indicating the strong "crack-curing" function of ACN as a rinsing solvent. The improved film quality indicates that the rinsing solvent ACN possesses "curing" capability for these cracks. This magical "solvent curing" effect may be partially attributed to the high dielectric constant (ε) of ACN. Recent progress of solution-phase ligand exchange for QDs has revealed that the electrostatically stabilized NCs are generally better dispersed in solvents with high dielectric constant due to effective screening of electrostatic attraction between oppositely charged ions.[28, 29] Therefore, dimethyl sulfoxide (DMSO) (ε≈47) and formamide (FA) (ε≈110) with very high ε values are often used as solvents to stabilize exchanged QDs. ACN (ε≈37.5) has a relatively higher dielectric constant than MeOH (ε≈32.5). We speculated that ACN could partially disperse iodide-exchanged PbS film and endowed the QDs certain mobility to reassemble and thus recover the cracks during the rinsing step. To verify this conjecture, the oleate-capped PbS QDs were dropped to the TBAI in methanol solution (same concentration as solid-state ligand exchange). After the exchange process completes, the solutions were centrifuged to remove the excess TBAI solution. Then the exchanged solid particles were dispersed in MeOH and ACN respectively. As shown in Figure S6, the iodide-exchanged PbS QDs were totally unable to disperse in MeOH, completely

precipitated in several minutes. In contrast, these PbS QDs could be dispersed in ACN and stabilized for at least several hours. These solutions were further centrifuged and the supernatant were collected and investigated. We found that the supernatant for the MeOH solvent was totally colorless without any residual PbS QDs. Conversely, the ACN supernatant displayed transparent brownish color, indicating certain solubility for iodide-exchanged PbS QDs. And this solution can keep stable for several weeks. However, the TBAI-exchanged PbS can hardly be dispersed in ACN after washed by MeOH, due to the loss of iodide ions on the QD surface (Figure S6c, S5d).[30] It is worth noting that when DMSO with a higher ε value than ACN was used as the rinsing solvent, the PbS-TBAI film was partially washed away from ITO/ZnO substrate (Figure S7) due to the too high solubility of iodide-exchanged PbS in DMSO. Thus, a proper ε value is one of the key criteria for the selection of rinsing solvents in the fabrication of PbS QDs solar cells.

The discovery of "solvent-curing" effect (schematically depicted in **Figure 5**a) can be utilized as a powerful tool to greatly reduce the complex film-deposition steps during the fabrication of QDs solar cells. Usually efficient PbS QDs solar cells using LbL solid-state ligand exchange method require around 10 deposition steps to avoid short circuit induced by cracks and to ensure satisfactory light absorption at the same time.[8] Thick layer and less LbL steps will often lead to increased number and sizes of cracks, resulting in reduced film quality and poor diode properties. Excitingly, using ACN as the rinsing solvent will help to simply the device fabrication process. As shown in Figure 5b and **Table 2**, devices fabricated with only 3 PbS-TBAI layers (photoactive layer) from 80 mg/mL PbS QDs (198±5 nm) can achieve a certified PCE of 11.21% (Figure 5c, Figure S8,9) and 11.84% for the lab champion device, which is the highest certified efficiency for PbX QDs photovoltaic devices using solid-state ligand exchange method to date. In contrast, the devices with conventional 5- photoactive layers only show a PCE of 10.66%. The better performance of device with less LbL steps may be attributed to the reduction of traps by decreasing total exposure time to offensive MeOH and

reducing the interfaces issues between each layer, which is consistent with its smaller diode ideality factor *n* from the light intensity dependence of V_{OC} (Figure S10). It is worth noting that the total thickness of the 3-photoactive layers (198±5 nm) prepared from 80 mg/mL PbS QDs is larger than that of the 5-photoactive layers (160±3 nm) prepared from 40 mg/mL PbS QDs (Table 2). To rigorously exclude the possible effect of film thickness, the "6-photoactive layers" device (PbS-TBAI: 195±5 nm) with the same thickness of the "3-photoactive layers" device was fabricated and only achieved similar PCE to that of the "5-photoactive layers" device (Figure S11, Table S3). The J_{SC} of "6-photoactive layers" device is higher than that of the "5-photoactive layers" device but similar to the "3-photoactive layers" device, which is in good agreement with the integrated J_{SC} values from external quantum efficiency (EQE) spectra (Figure S12). The results exclude the effect of film thickness and confirmed the apparent advantage of using less LbL steps. MeOH-rinsed device with 3 photoactive layers was also fabricated and shows much lower PCE than that of the ACN-rinsed 3-photoavtive layer device, resulting from increased traps and worse film morphology. Compared to MeOH-rinsed 5-photoactive layers device, MeOH-rinsed 3-layers device has slightly better device performance (Figure S13, Table S4), likely due to reduced total exposure time to MeOH during ligand exchange and rinsing processing. To further reduce the LbL steps, we fabricated 2-photoactive layers devices using 120 mg/mL QDs solution to maintain similar total film thickness. We still managed to obtain a high PCE of 10.60% for ACN-rinsed device, as shown in Table 2. Comparing to the ACN-rinsed 3-photoactive layers device, the overall reduced photovoltaic parameters of 2-photoactive layers devices can be ascribed to the larger cracks generated in a thicker single film, which may not be fully repaired by ACN rinsing (Figure S5f). It is worth noting that with much simplified structure, the PCE of ACN-rinsed 2-photoactive layers device is still comparable to that of the "5- photoactive layers" device, and much better than the corresponding MeOH-rinsed 2-photoactive layers device. However, ultimately reducing to 1-photoactive layer from a more concentrated 200 mg/mL PbS solution resulted in huge cracks

across the whole film (Figure S14), which has exceeded the curing capacity of ACN, leading to a low PCE of 1-3% and poor reproducibility. Herein, it can be concluded that traps reduction plays an important role on the performance for the device with high-quality film while film curing is vital for the device with large-cracks PbS-TBAI layers. Nonetheless, it can be expected that further optimization on both ligand exchange and rinsing processing will boost the development of highly efficient QDs solar cells with less or even single layer deposition, which is critical for the low-cost large-area photovoltaic device.

In summary, due to the aprotic nature of ACN, less trap states are introduced during the rinsing process compared to the conventional rinsing solvent MeOH. Better device performance was achieved by using ACN as the rinsing solvent after ligand exchange. Meanwhile, it was discovered for the first time that ACN possesses a "film-curing" capability when employed as the rinsing solvent during the fabrication of PbS QDs solar cells. Its high dielectric value provides certain mobility to the ligand-exchanged QDs and allows the re-assembling of QDs in film to cure the cracks generated during solid ligand-exchange processing. More importantly, utilizing the "film-curing" function of ACN can greatly simplify the complex film deposition processing normally required in PbS QDs solar cells while achieving higher PCE at the same time. As a result of reduced traps and improved film quality, a certified solar AM1.5G power-conversion efficiency of 11.21% (lab champion PCE of 11.84%) was achieved with only 3 deposition steps for the photoactive layers, which is the highest certified/reported efficiency to date for PbX QDs photovoltaic devices using the solid-state ligand exchange method. Our results provide a facile and reliable approach to achieve high-performance PbS QDs solar cells with largely simplified deposition processing. We believe further optimization on both ligand exchange and rinsing processing will allow single layer deposition and facilitate scalable manufacturing of large-area photovoltaic devices.

Experimental Section

Synthesis of colloidal PbS QDs: The oleate-capped PbS QDs were synthesized via a rapid hot injection method by following a reported procedure.[31] Briefly, 10 mmol of lead acetate trihydrate and 7 g of oleic acid (OA) were dissolved in 60 g of 1-octadecene (ODE) in a three-neck flask by heating the mixture to 100 °C under vacuum for 2 hours. The sulfur precursor was prepared separately by mixing 1 mL of hexamethyldisilathiane and 9 mL of 1-octadecene. The reaction was initiated by rapid injection of the sulfur precursor into the lead precursor solution at 75 °C under nitrogen. The QDs were grown at this temperature for 10 min and then cooled to room-temperature slowly. The solution was then transferred into a nitrogen-filled glovebox and purified by precipitation twice in hexane/isopropyl alcohol and once in hexane/acetone. The PbS QDs were stored with solid form in nitrogen-filled glovebox.

Synthesis of ZnO nanoparticles: ZnO nanoparticles were synthesized according to our previous work.[32] Zinc acetate dihydrate (2.95 g) was dissolved in methanol (125 mL) at 63.5 °C. Potassium hydroxide (1.48 g) was dissolved in methanol (65 mL). The potassium hydroxide solution was slowly added to the zinc acetate solution then the solution was kept stirring at 63.5 °C for 3 h. ZnO nanocrystals were extracted by centrifugation and then washed twice by methanol followed by centrifugation. Finally, 10 mL of chloroform and 10 mL methanol were added to the precipitates and the solution was filtered with a 0.45 μm filter.

Device Fabrication: The ITO-coated glass substrate was ultrasonically cleaned with solvents and then treated with oxygen plasma. ZnO layers (80 nm) were fabricated by spin-coating a solution of ZnO nanoparticles onto ITO. PbS QD layers were fabricated by LbL spin-coating. For 5-photoactive layers device, ~30 μl of a 40 mg/mL solution of PbS QDs in hexane was spin-cast onto the substrate at 2500 rpm for 10 s. A TBAI solution (10 mg/mL in methanol) was applied to the substrate for 30 s, followed by two rinse-spin steps with MeOH or ACN. For

3, 2, 1-photoactive-layers device, the process of fabricating PbS-TBAI layer were similar with different PbS concentration (80 mg/mL, 120 mg/mL, 200 mg/mL), different TBAI concentration (20 mg/mL, 25 mg/mL, 30 mg/mL) and different ligand-exchange time (40 s, 60 s, 100 s) respectively. For the two PbS-EDT layers, a PbS solution (20 mg/mL in hexane), an EDT solution (0.04 vol% in ACN) and ACN were used. All the spin-coating steps were performed under ambient condition and at room temperature. The films were stored in air overnight and then transferred to a nitrogen-filled glovebox for electrode evaporation. Au (100 nm thick) were deposited by thermal evaporation through a shadow mask at a reduced pressure ($< 10^{-6}$ Torr).

Measurement and characterization: The current density–voltage characteristics of the photovoltaic cells were measured using a Keithley 2400 (*I*–*V*) digital source meter under a simulated AM 1.5G solar irradiation at 100 mW/cm^2 (Newport, Class AAA solar simulator, 94023A-U). The light intensity is calibrated by a certified Oriel Reference Cell (91150V) and verified with a NREL calibrated Hamamatsu S1787-04 diode. The area listed in the certified result is determined by sample outer range with optical microscope. EQE measurements were conducted using a certifed IPCE instrument (Zolix Instruments, Inc, Solar Cell Scan100). The transient photovoltage decay spectroscopies were tested by a pulse laser light source (532 nm) under white light bias, and signals were recorded on Tektronix oscilloscope. Field-effect transistor measurements were carried out on a Keithley semiconductor characterization system 4200-SCS in combination with a probe station in nitrogen-filled glovebox. The capacitance-voltage measurements were acquired with Keithley 4200-CVU semiconductor characterization system with the samples stored in a high vacuum (~10^{-6} Torr) probe station at a frequency of 50 kHz and an AC signal of 100 mV, scanning from -1 to 1 V. Photoluminescence measurements were performed on samples prepared on quartz substrates by spin-coating 5 layers of PbS QDs with different washing methods. The second harmonic (400 nm) of a

Ti:sapphire laser (Coherent, Mira 900, repetition rate 76 MHz) was used to excite the samples. The optical emission was recorded by a cooled array detector (Andor, iDus 1.7 μm). Time-resolved PL spectra were detected using a Hamamatsu streak camera with a cathode sensitive to near-IR radiation. X-ray photoelectron spectroscopy (XPS) was carried out in a SPECSTM ultrahigh vacuum photoelectron spectroscopy system. The scanning electron microscopy (SEM) image were characterized on a Zeiss Supra 55 field in high vacuum mode at 20 kV accelerating voltages. SEM cross sections were prepared by a Carl Zeiss Auriga 60 FIB/SEM with a 30 kV voltage beam at 50 pA. Cross-sectional SEM images were taken at 5 kV and 30 μm aperture size using an in-lens detector. UV-Vis-NIR spectra were recorded on a Perkin Elmer model Lambda 750.

Supporting Information

Supporting Information is available from the Wiley Online Library or from the author.

Acknowledgements

The authors acknowledge financial support from the National Key Research and Development (R&D) Program of China (Grant No. 2016YFA0202402), the National Natural Science Foundation of China (Grant No. 61674111) and the Natural Science Foundation of Jiangsu Province of China (BK20170337). The authors also thank financial support from the "111" projects. This project is also funded by the Collaborative Innovation Center of Suzhou Nano Science and Technology (Nano-CIC), Soochow University and by the Priority Academic Program Development of Jiangsu Higher Education Institutions (PAPD). X. Ye acknowledges startup fund from Indiana University. Z. Liu thanks National Postdoctoral Program for Innovative Talents (Grant No. BX201600113) and Postdoctoral Science Foundation of China (Grant No.2017M610349). The authors kindly thank Ryan P. Borman for useful discussions. K. Lu and Y. Wang contributed equally to this work.

Received: ((will be filled in by the editorial staff))
Revised: ((will be filled in by the editorial staff))
Published online: ((will be filled in by the editorial staff))

References

[1] Z. Liu, J. Yuan, S. A. Hawks, G. Shi, S.-T. Lee and W. Ma, *Solar RRL*, **2017**, *1*, 1600021.

[2] G. H. Carey, A. L. Abdelhady, Z. Ning, S. M. Thon, O. M. Bakr and E. H. Sargent, *Chem. Rev.*, **2015**, *115*, 12732-12763.

[3] C. R. Kagan and C. B. Murray, *Nat. Nano.*, **2015**, *10*, 1013-1026.

[4] R. Saran and R. J. Curry, *Nat. Photon.*, **2016**, *10*, 81-92.

[5] M. Liu, O. Voznyy, R. Sabatini, F. P. Garcia de Arquer, R. Munir, A. H. Balawi, X. Lan, F. Fan, G. Walters, A. R. Kirmani, S. Hoogland, F. Laquai, A. Amassian and E. H. Sargent, *Nat. Mater.*, **2017**, *16*, 258-263.

[6] C. H. Chuang, P. R. Brown, V. Bulovic and M. G. Bawendi, *Nat. Mater.*, **2014**, *13*, 796-801.

[7] G. Shi, Y. Wang, Z. Liu, L. Han, J. Liu, Y. Wang, K. Lu, S. Chen, X. Ling, Y. Li, S. Cheng and W. Ma, *Adv. Energy Mater.*, **2017**, DOI: 10.1002/aenm.201602667.

[8] R. Wang, Y. Shang, P. Kanjanaboos, W. Zhou, Z. Ning and E. H. Sargent, *Energy Environ. Sci.*, **2016**, *9*, 1130-1143.

[9] J. M. Luther, M. Law, M. C. Beard, Q. Song, M. O. Reese, R. J. Ellingson and A. J. Nozik, *Nano lett.*, **2008**, *8*, 3488-3492.

[10] G. I. Koleilat, L. Levina, H. Shukla, S. H. Myrskog, S. Hinds, A. G. Pattantyus-Abraham and E. H. Sargent, *ACS nano*, **2008**, *2*, 833-840.

[11] A. G. Pattantyus-Abraham, I. J. Kramer, A. R. Barkhouse, X. Wang, G. Konstantatos, R. Debnath, L. Levina, I. Raabe, M. K. Nazeeruddin, M. Grätzel and E. H. Sargent, *ACS Nano*, **2010**, *4*, 3374-3380.

[12] K. S. Jeong, J. Tang, H. Liu, J. Kim, A. W. Schaefer, K. Kemp, L. Levina, X. Wang, S. Hoogland, R. Debnath, L. Brzozowski, E. H. Sargent and J. B. Asbury, *ACS Nano*, **2012**, *6*, 89-99.

[13] J. Tang, H. Liu, D. Zhitomirsky, S. Hoogland, X. Wang, M. Furukawa, L. Levina and E. H. Sargent, *Nano Lett.*, **2012**, *12*, 4889-4894.

[14] X. Lan, O. Voznyy, A. Kiani, F. P. Garcia de Arquer, A. S. Abbas, G. H. Kim, M. Liu, Z. Yang, G. Walters, J. Xu, M. Yuan, Z. Ning, F. Fan, P. Kanjanaboos, I. Kramer, D. Zhitomirsky, P. Lee, A. Perelgut, S. Hoogland and E. H. Sargent, *Adv. Mater.*, **2016**, *28*, 299-304.

[15] X. Lan, O. Voznyy, F. P. García de Arquer, M. Liu, J. Xu, A. H. Proppe, G. Walters, F. Fan, H. Tan, M. Liu, Z. Yang, S. Hoogland and E. H. Sargent, *Nano Lett.*, **2016**, *16*, 4630-4634.

[16] M. Liu, F. P. de Arquer, Y. Li, X. Lan, G. H. Kim, O. Voznyy, L. K. Jagadamma, A. S. Abbas, S. Hoogland, Z. Lu, J. Y. Kim, A. Amassian and E. H. Sargent, *Adv. Mater.*, **2016**, *28*, 4142-4148.

[17] A. R. Kirmani, G. H. Carey, M. Abdelsamie, B. Yan, D. Cha, L. R. Rollny, X. Cui, E. H. Sargent and A. Amassian, *Adv. Mater.*, **2014**, *26*, 4717–4723.

[18] A. Hassinen, I. Moreels, K. De Nolf, P. F. Smet, J. C. Martins and Z. Hens, *J. Am. Chem. Soc.*, **2012**, *134*, 20705-20712.

[19] Z. Ning, O. Voznyy, J. Pan, S. Hoogland, V. Adinolfi, J. Xu, M. Li, A. R. Kirmani, J. P. Sun, J. Minor, K. W. Kemp, H. Dong, L. Rollny, A. Labelle, G. Carey, B. Sutherland, I.

Hill, A. Amassian, H. Liu, J. Tang, O. M. Bakr and E. H. Sargent, *Nat. Mater.*, **2014**, *13*, 822-828.

[20] J. H. Song, H. Choi, Y.-H. Kim and S. Jeong, *Adv. Energy Mater.*, **2017**, DOI: 10.1002/aenm.201700301.

[21] D. M. Balazs, D. N. Dirin, H. H. Fang, L. Protesescu, G. H. ten Brink, B. J. Kooi, M. V. Kovalenko and M. A. Loi, *ACS Nano*, **2015**, *9*, 11951-11959.

[22] C. H. Chuang, A. Maurano, R. E. Brandt, G. W. Hwang, J. Jean, T. Buonassisi, V. Bulovic and M. G. Bawendi, *Nano Lett.*, **2015**, *15*, 3286-3294.

[23] M. J. Speirs, D. N. Dirin, M. Abdu-Aguye, D. M. Balazs, M. V. Kovalenko and M. A. Loi, *Energy Environ. Sci.*, **2016**, *9*, 2916-2924.

[24] M. Zhao, F. Yang, C. Liang, D. Wang, D. Ding, J. Lv, J. Zhang, W. Hu, C. Lu and Z. Tang, *Adv. Funct. Mater.*, **2016**, *26*, 5182–5188.

[25] C. Ammon, A. Bayer, G. Held, B. Richter, T. Schmidt and H. P. Steinrück, *Surf. Sci.*, **2002**, *507-510*, 845-850.

[26] C. J. Weststrate, W. Ludwig, J. W. Bakker, A. C. Gluhoi and B. E. Nieuwenhuys, *J. Phys. Chem. C*, **2007**, *111*, 7741-7747.

[27] J. M. Luther, M. Law, Q. Song, C. L. Perkins, M. C. Beard and A. J. Nozik, *ACS Nano*, **2008**, *2*, 271-280.

[28] A. Nag, M. V. Kovalenko, J. S. Lee, W. Liu, B. Spokoyny and D. V. Talapin, *J. Am. Chem. Soc.*, **2011**, *133*, 10612–10620.

[29] M. A. Boles, D. Ling, T. Hyeon and D. V. Talapin, *Nat. Mater.*, **2016**, *15*, 141-153.

[30] Z. Ning, H. Dong, Q. Zhang, O. Voznyy, and E. H. Sargent, *ACS Nano*, **2014**, *8*, 10321-10327

[31] M. A. Hines and G. D. Scholes, *Adv. Mater.*, **2003**, *15*, 1844-1849.

[32] G. Shi, Y. Wang, Z. Liu, L. Han, J. Liu, Y. Wang, K. Lu, S. Chen, X. Ling, Y. Li, S. Cheng and W. Ma, *Adv. Energy Mater.*, **2017**, DOI: 10.1002/aenm.201602667.

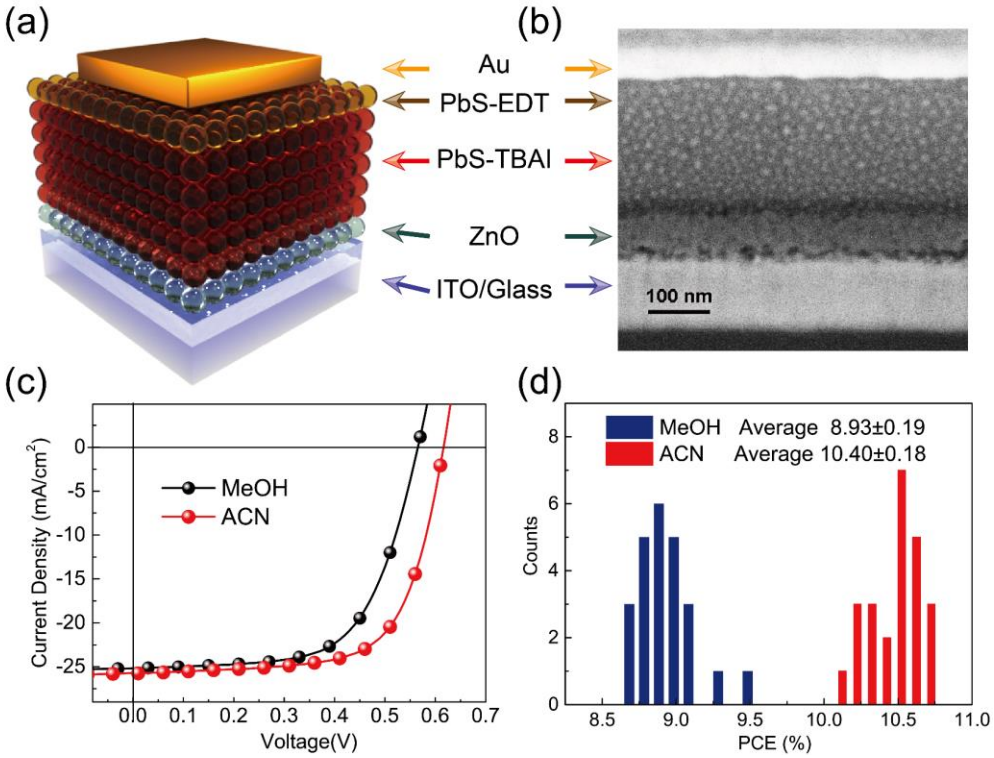

Figure 1. (a) Schematic diagram of the PbS QDs photovoltaic device used in this study. (b) Cross-sectional SEM image of the PbS QDs device. (c) Current-voltage characteristics, (d) PCE histograms of the 5-photoactive layers PbS QDs devices rinsed by MeOH and ACN.

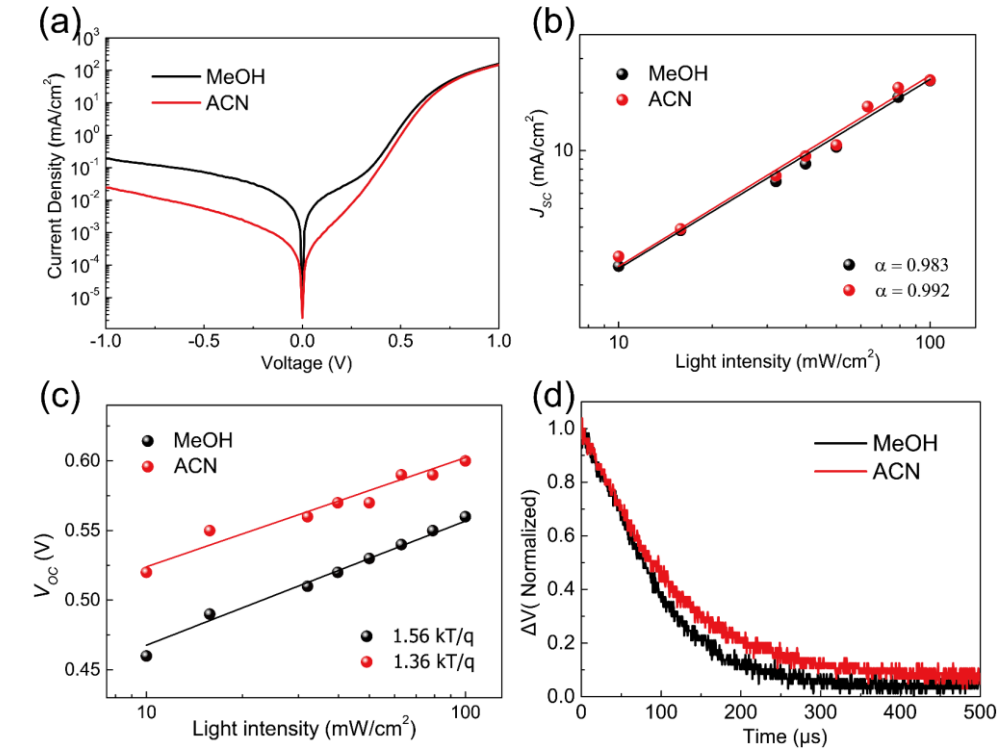

Figure 2. (a) Dark *J-V* curve, (b) light-intensity dependence of J_{SC} (Solid lines: linear fits), (c) light intensity dependence of V_{OC} (Solid lines: linear fits), (d) transient photovoltage decay spectroscopy of the 5-photoactive layers PbS QDs devices rinsed by MeOH and ACN.

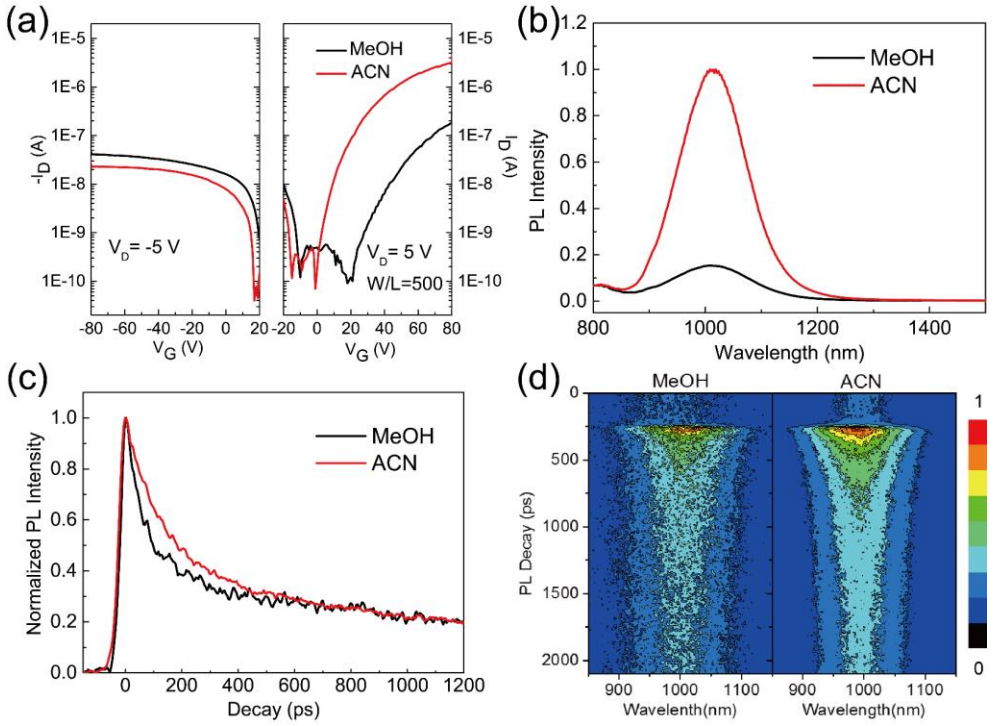

Figure 3. (a) P-channel (left) and n-channel (right) transfer curves of FETs prepared with PbS-TBAI layers rinsed by MeOH and ACN. (b) Steady-state fluorescence, (c) time-resolved fluorescence spectra and (d) 2D transient PL decay of PbS-TBAI film rinsed by MeOH and ACN.

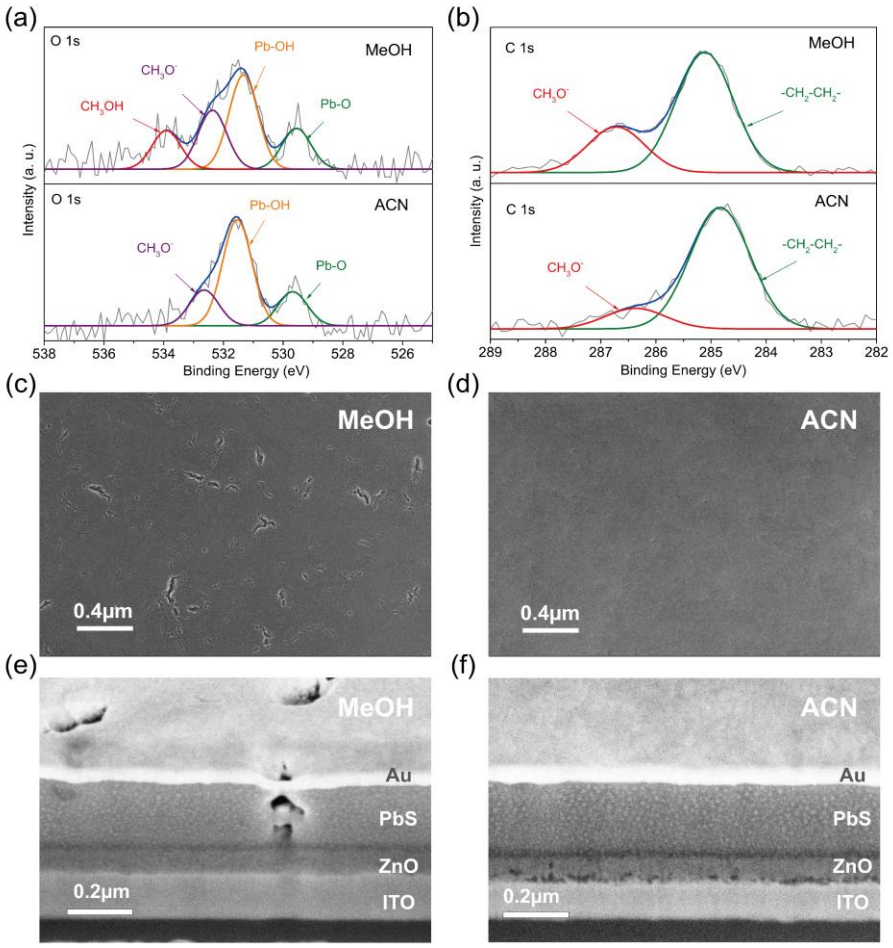

Figure 4. High-resolution XPS spectra of PbS-TBAI films rinsed by MeOH and ACN: (a) O 1s; (b) C 1s. SEM images for one-layer TBAI-exchanged PbS (80 mg/mL) film, rinsed by (c) MeOH and (d) ACN. Cross-sectional SEM images of the samples (ITO/ZnO/PbS (80 mg/mL)-TBAI×3/PbS-EDT×2/Au) with PbS-TBAI layers rinsed by MeOH (e) and ACN (f).

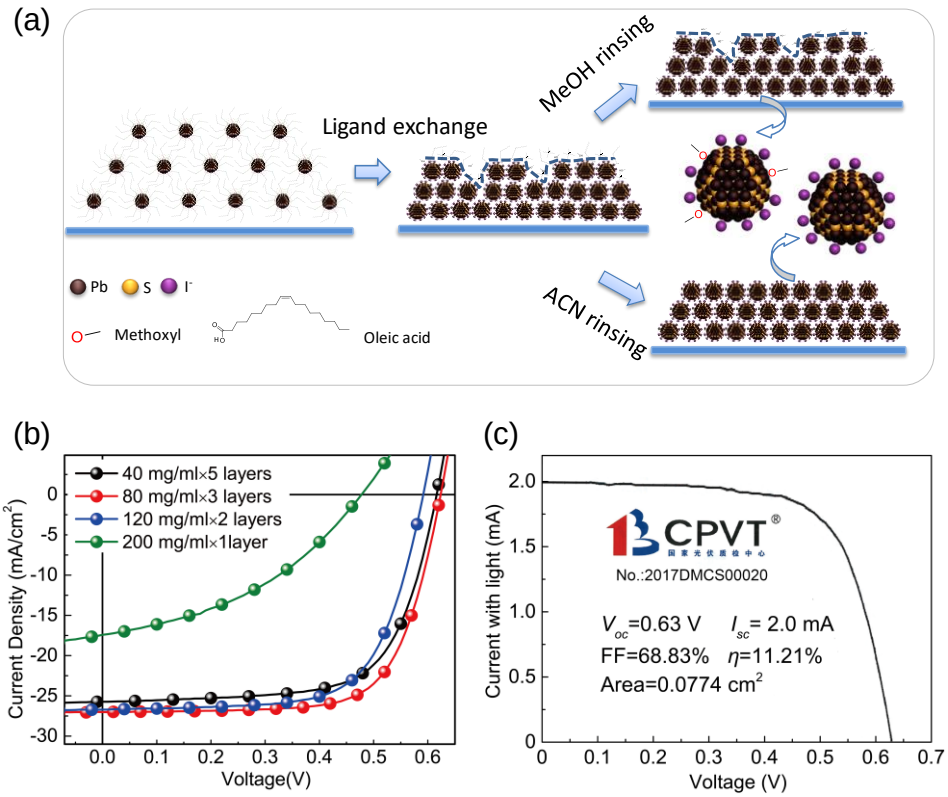

Figure 5. (a) Schematic diagram of the effect of rinsing solvents on film morphology. (b) Current-voltage characteristic of PbS QDs solar cells with different numbers of photoactive layers prepared from PbS QDs with different concentrations. The rinsing solvents are all ACN. (c) Current-voltage characteristic of certified PbS QDs solar cells based on 3-photoactive layers.

Table 1. Device parameters of the PbS QDs solar cells (ITO/ZnO/PbS-TBAI×5/PbS-EDT×2/Au) with PbS-TBAI layers rinsed by MeOH and ACN. (The numbers in parentheses represent the values obtained from the best-performing cell.)

	V_{OC} (V)	J_{SC} (mA/cm^2)	FF (%)	PCE (%)
MeOH rinsing	0.556±0.015 (0.56)	25.12±0.64 (25.01)	64.0±1.5 (67.3)	8.93±0.19 (9.43)
ACN rinsing	0.602±0.009 (0.61)	25.18±0.63 (25.73)	68.6±1.6 (67.9)	10.40±0.18 (10.66)

Table 2. Device parameters of PbS QDs solar cells with different numbers of photoactive layers. The rinsing solvents are all ACN. (The numbers in parentheses represent the values obtained from the best-performing cell.)

PbS-TBAI	V_{OC} (V)	J_{SC} (mA/cm^2)	FF (%)	PCE (%)
40 mg/mL× 5 layers /160±3 nm	0.602±0.009(0.61)	25.18±0.63(25.73)	68.6±1.6(67.9)	10.40±0.18(10.66)
80 mg/mL×3 layers /198±5nm	0.615±0.009(0.62)	26.36±0.73(27.08)	70.1±0.4(70.5)	11.32±0.31(11.84)
80 mg/mL × 3 layers /certified	0.63	25.84	68.8	11.21
120 mg/mL × 2 layers /220±7nm	0.580±0.012(0.59)	24.59±1.41(26.70)	65.6±3.7(67.3)	9.38±1.13(10.60)
200 mg/mL × 1 layer /249±30nm	0.253±0.11(0.47)	13.95±2.39(17.33)	34.2±3.9(40.8)	1.34±0.88(3.32)

The table of contents entry

A certified PCE of 11.21% (lab champion PCE of 11.84%) for PbS colloidal quantum dot (CQD) solar cells was achieved with only 3 deposition steps for the photoactive layers, benefiting from the "film-curing" function of ACN as rinsing solvent.

Keywords: Solar Cells, PbS Quantum Dots, Rinsing Solvent, Solvent-Curing

K. Lu, Y. Wang, Z. Liu, L. Han, G. Shi, H. Fang, J. Chen, Prof. X. Ye, S. Chen, F. Yang, A. G. Shulga T. Wu, M. Gu, S. Zhou, Prof. J. Fan, Prof. M. A. Loi* and Prof. W. Ma*

High-Efficiency PbS Quantum Dots Solar Cells with Greatly Simplified Fabrication Processing via "Solvent-Curing"

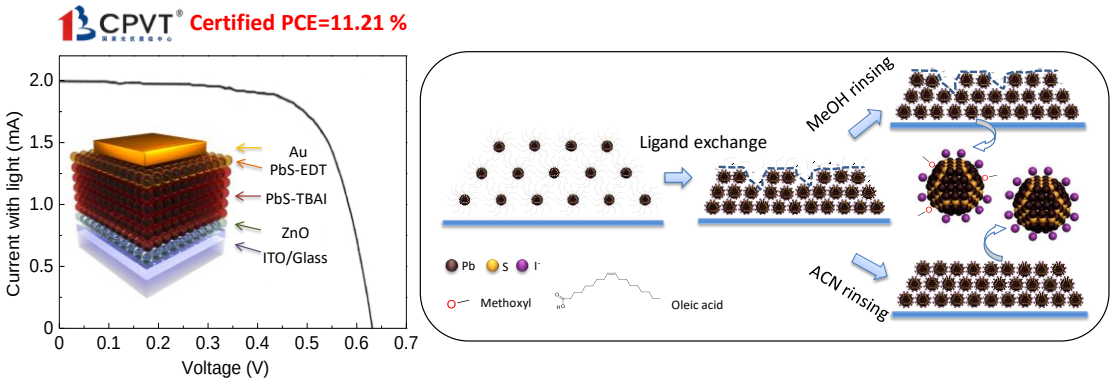

Supporting Information

High-Efficiency PbS Quantum Dots Solar Cells with Greatly Simplified Fabrication Processing via "Solvent-Curing"

Kunyuan Lu,‡ Yongjie Wang,‡ Zeke Liu, Lu Han, Guozheng Shi, Honghua Fang, Jun Chen, Xingchen Ye, Si Chen, Fan Yang, Artem G. Shulga, Tian Wu, Mengfan Gu, Sijie Zhou, Jian Fan, Maria Antonietta Loi and Wanli Ma**

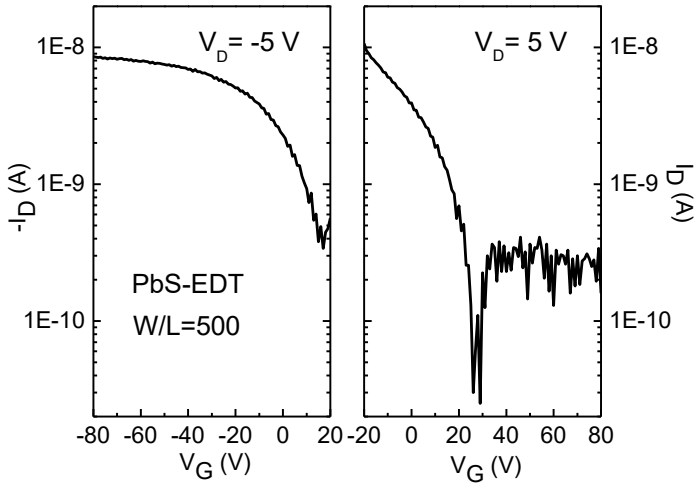

Figure S1. FETs Transfer curves of PbS-EDT layer.

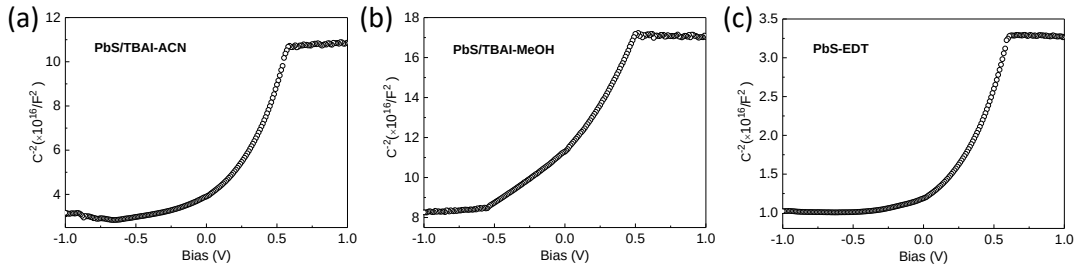

Figure S2. Capacitance Voltage Measurements for PbS-TBAI film rinsed with (a) ACN; (b) MeOH and (c) PbS-EDT film. All the devices are with a structure of ITO/PbS/Au.

The Schottky plot (C^{-2} vs. V) is used to estimate the doping density of the n-type PbS QDs based on a n-p^{++} approximation and the p-type PbS QDs based on a n^{++}-p approximation. The doping density (*N*) was calculated using the slope of plot.

$$\frac{1}{C^2} = \frac{2V}{qNA^2\varepsilon_0\varepsilon_r}$$

C = capacitance of the space charge region (depletion region)

ε_0 = permittivity of free space

ε_r = dielectric constant of the PbS CQDs (18.7 for PbS-TBAI, 18 for PbS-EDT)[S2]

N = doping density

A = area

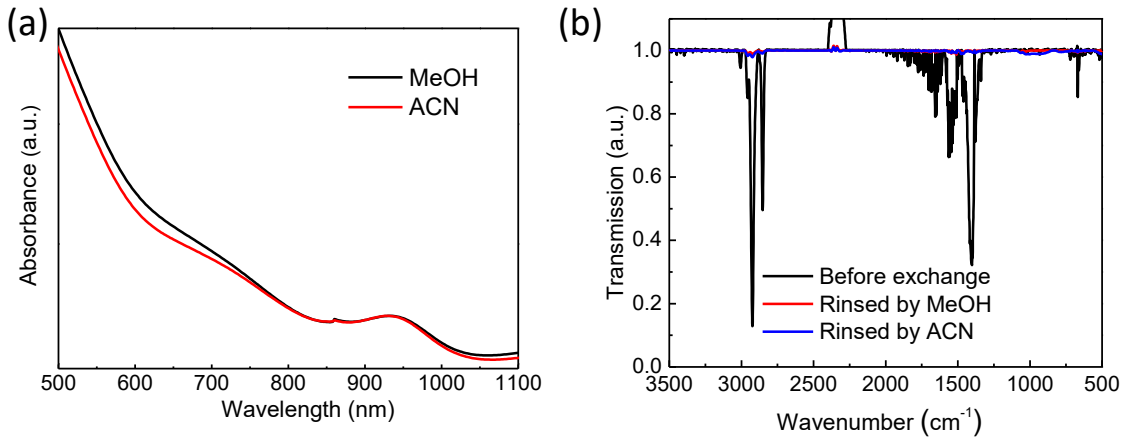

Figure S3. (a) Absorbance spectra of PbS-TBAI films rinsed by MeOH and ACN. (b) FTIR spectra for PbS QDs films (Before exchange; PbS-TBAI films rinsed by MeOH and ACN).

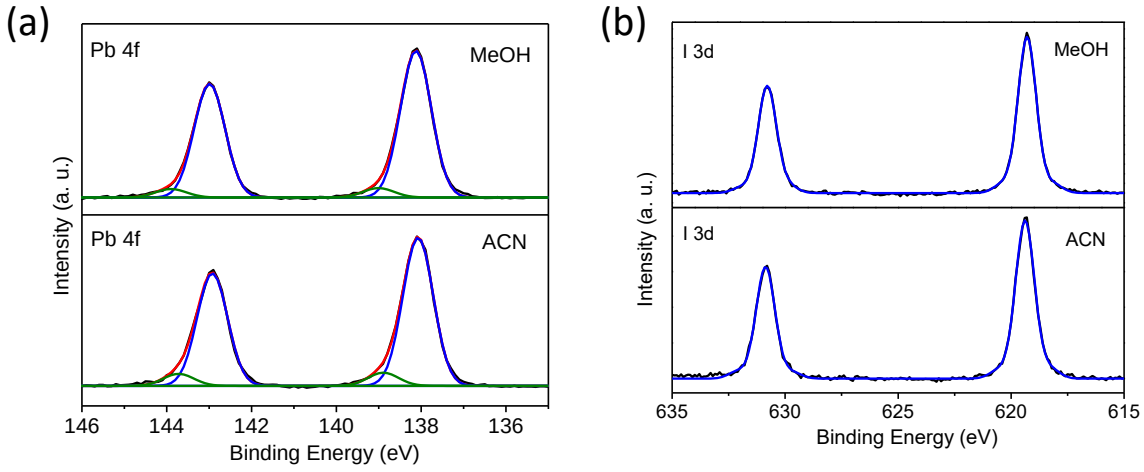

Figure S4. XPS spectra of PbS-TBAI films rinsed by MeOH and ACN: (a) Pb 4f; (b) I 3d.

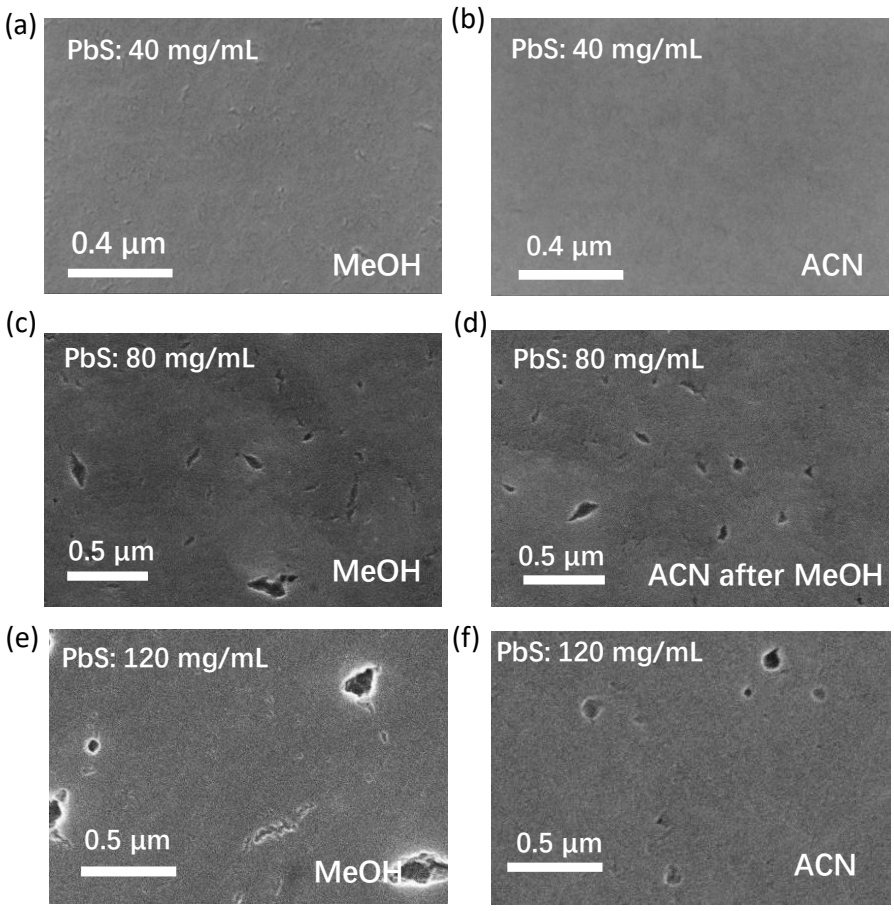

Figure S5. SEM images for TBAI exchanged PbS QDs film with different QDs concentrations and rinsing conditions.

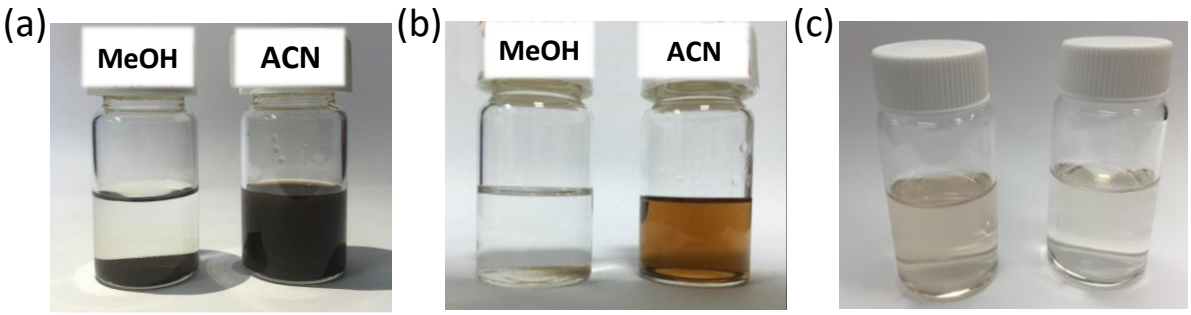

Figure S6. (a) Photographs of TBAI-exchanged PbS QDs dispersed in MeOH and ACN respectively. (b) The corresponding supernatant after centrifugation for the samples in (a).(c) The supernatant of TBAI-exchanged PbS QDs dispersed in ACN after one time (left) and twice (right) washing with MeOH. It clearly shows TBAI-exchanged PbS QDs will gradually lose their dispersibility in ACN after purification, due to the lost of surface ions.

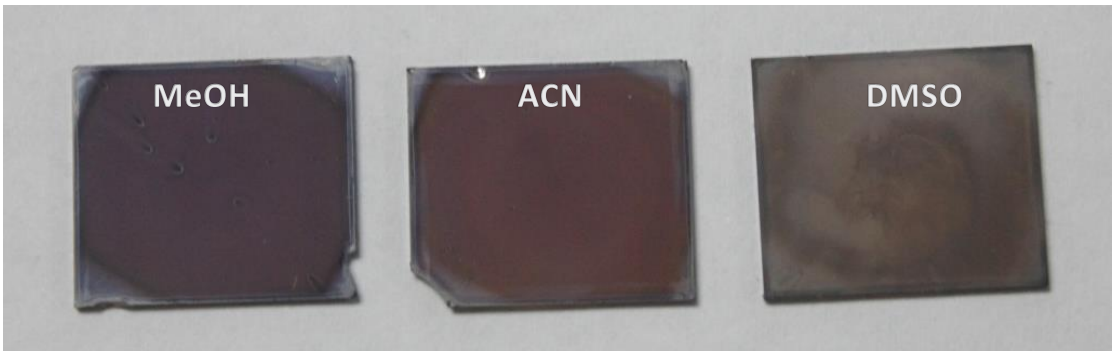

Figure S7. Photographs of 3-layer TBAI-exchanged PbS (80 mg/mL) films, rinsed by MeOH, ACN and DMSO

CPVT®
国家光伏质检中心

TEST REPORT

No.:2017DMCS00020

PRODUCT NAME	Solar cell
TYPE/MODEL	Lead Sulfide Quantum dots solar cells
CUSTOMER	Soochow University

National Center of Supervision & Inspection on Solar Photovoltaic Products Quality

Figure S8a. Cover page of test for a "3- photoactive layers" PbS QDs solar cell (China Photovoltaic Test, CPVT) report by National Center of Supervision and Inspection on Solar Photovoltaic Product Quality.

Test Results

No:2017DMCS00020 Page 4 of 5

Clause	Test item(s)	Unit	Technical requirements	Results	Verdict Pass/Fail
1	Current-voltage characteristic measurement (1#)	---	At STC (module temperature: 25 ℃, irradiance: 1000W/m², standard solar spectral irradiance distribution corresponds to IEC60904-3), measure the current-voltage characteristics of the cell with the variation of load	------	---
1.1	Open-circuit voltage, Voc	V	------	0.6300	---
1.2	Short-circuit current, Isc	mA	------	2.000	---
1.3	Maximun-power, Pmax	mW	------	0.8673	---
1.4	Maximun-power voltage, Vmp	V	------	0.4900	---
1.5	Maximun-power current, Imp	mA	------	1.770	---
1.6	Fill factor, F.F. (%)	---	------	68.83	---
1.7	Calculate conversion efficiency	---	------	---	---
1.7.1	Conversion efficiency, η (%)	---	$\eta = \frac{Pmax}{1000W/m^2 \times S} \times 100\%$	11.21	---
1.7.2	Area, S	cm²	S is determined by sample surface outer range	0.0774	---

1# - Current-voltage characteristic at STC

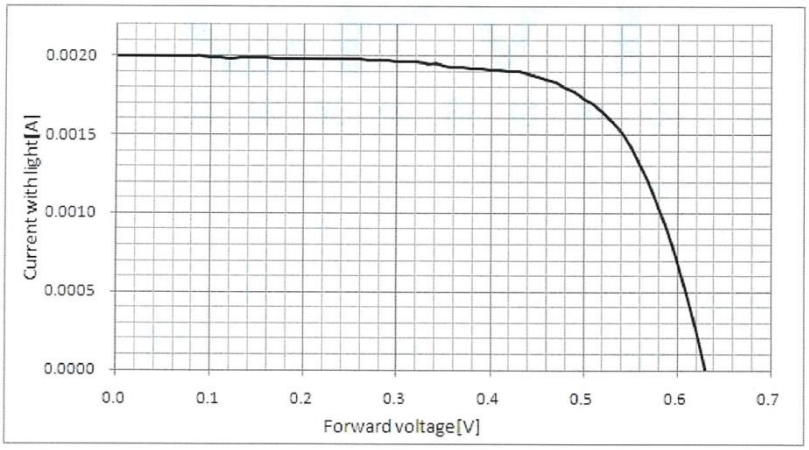

Remark: ------

Figure S8b. Certified PCE for a "3- photoactive layers" PbS QDs device as measured by National Center of Supervision and Inspection on Solar Photovoltaic Product Quality.

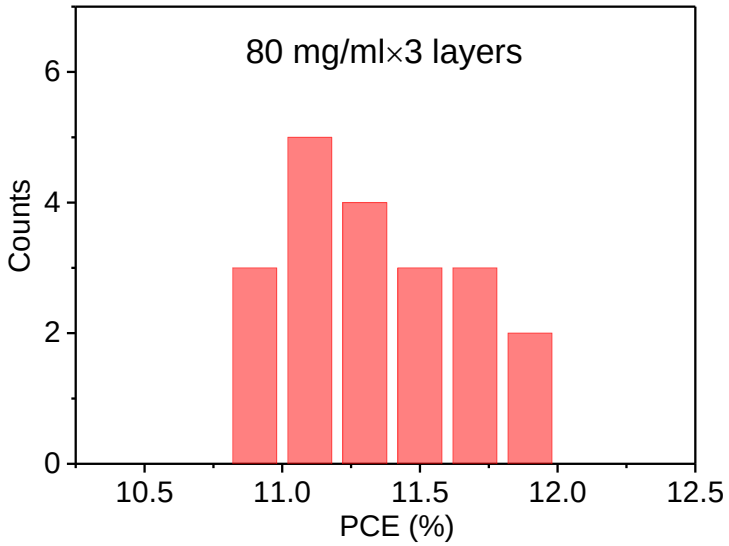

Figure S9. PCE histogram of solar cells deposited with 3 photoactive layers PbS (80 mg/mL) QDs device (ITO/ZnO/PbS-TBAI×3/PbS-EDT×2/Au).

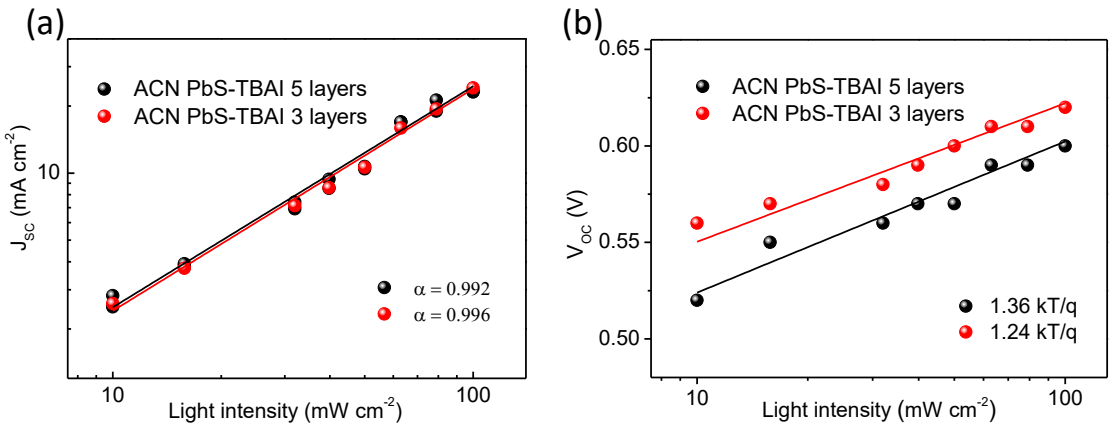

Figure S10. (a) Light-intensity dependence of J_{sc} (Solid lines: linear fits) (b) Light intensity dependence of V_{oc} (Solid lines: linear fits) of the PbS QDs device with PbS(40mg/mL)-TBAI×5 layers and PbS(80mg/mL)-TBAI×3 layers.

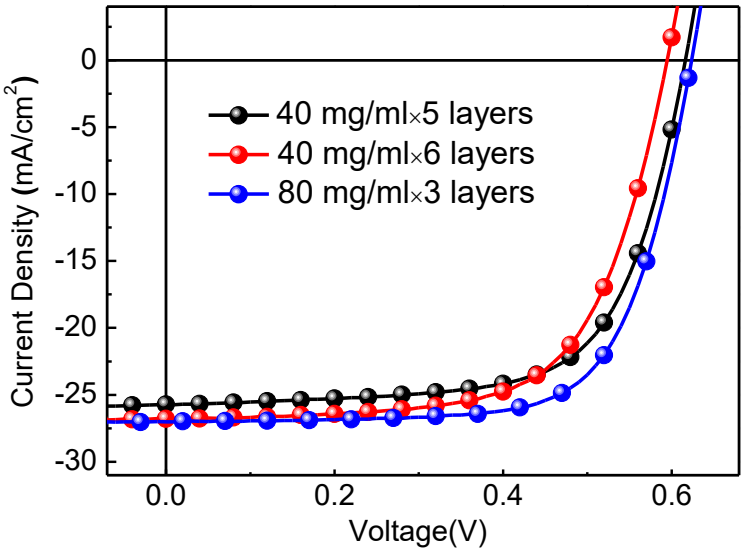

Figure S11. Current-voltage characteristics of PbS QDs solar cells with different numbers of photoactive layers prepared from PbS QDs with different concentrations. The rinsing solvents are all ACN.

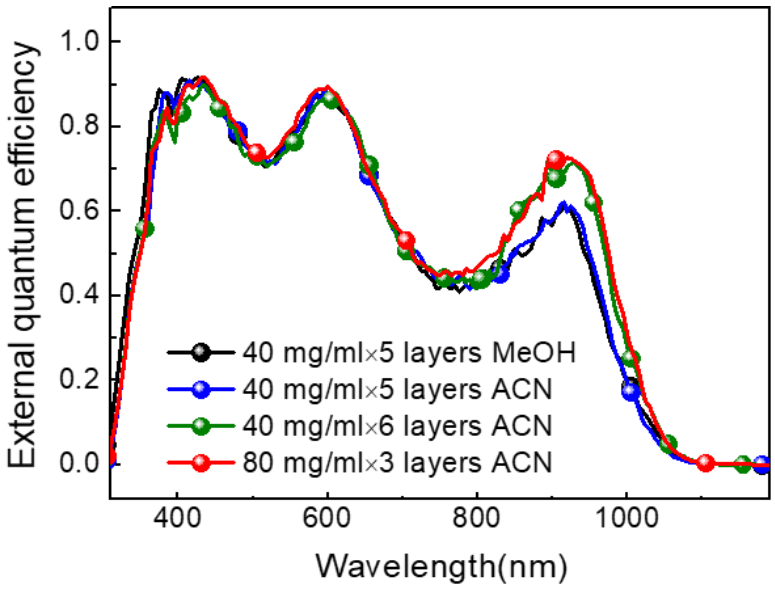

Figure S12. EQE spectra of devices with different deposition conditions. The calculated J_{SC} values from EQE spectra of the devices "40 mg/ml×5 layers MeOH", "40 mg/ml×5 layers ACN", "40 mg/ml×6 layers ACN", "80 mg/ml×3 layers ACN" are 24.33 mA/cm^2, 24.27 mA/cm^2, 25.18 mA/cm^2 and 25.68 mA/cm^2, respectively. Compared to the *J–V* characteristics J_{SC} values: 25.12 mA/cm^2, 25.18 mA/cm^2, 26.80 mA/cm^2, 27.08 mA/cm^2, the errors are 3.14%, 3.61%, 6.04% and 5.17% respectively, showing good agreement with the EQE results.

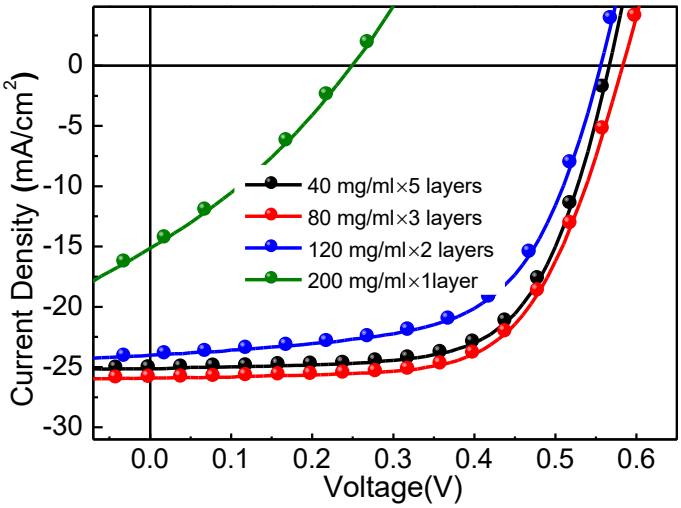

Figure S13. Current-voltage characteristic of PbS QDs solar cells with different numbers of photoactive layers prepared from PbS QDs with different concentrations. The rinsing solvents are all MeOH.

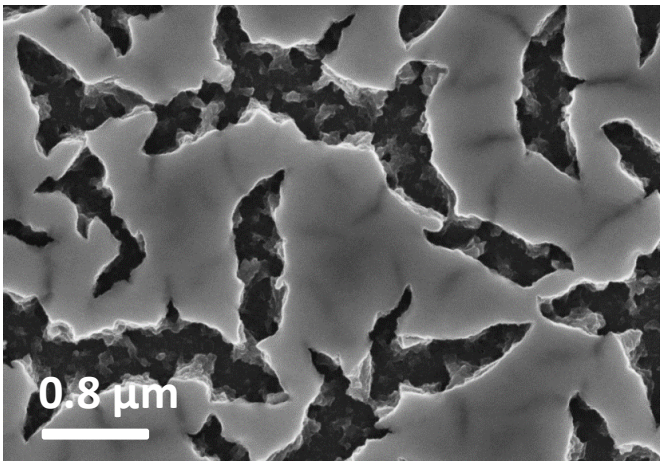

Figure S14. SEM images for one-layer TBAI-exchanged PbS film rinsed by ACN. (Processed from PbS 200 mg/mL in hexane).

Table S1. Summary of mobility and doping density for different layers. These values are close to the previously reported values with the same fabrication conditions. [1,2]

	Mobility ($cm^2 V^{-1} s^{-1}$)	**Doping density** (cm^{-3})
TBAI/ACN	$1.7X10^{-3}$ (electron)	$5.87X10^{16}$
TBAI/MeOH	$1.6X10^{-4}$ (electron)	$8.51X10^{16}$
EDT	$3.9X10^{-6}$ (hole)	$2.39X10^{17}$

Table S2. Lifetime and fractional contribution of different photoluminescence decay channels for PbS-TBAI films rinsed by MeOH and ACN.

	τ_1 (ps)	τ_2 (ps)	Amplitude 1	Amplitude 2
MeOH	74.4	2185.4	0.69	0.31
ACN	139.1	2185.0	0.68	0.33

Table S3. Device parameters of PbS QDs solar cells with different photoactive layers. The rinsing solvent are all ACN.

PbS-TBAI	V_{OC} (V)	J_{SC} (mA/cm^2)	FF (%)	PCE (%)
40 mg/ml×5 layers /160±3 nm	0.61	25.73	67.9	10.66
40 mg/ml × 6 layers /195±5 nm	0.59	26.80	65.9	10.41
80 mg/ml × 3 layers /198±5nm	0.62	27.08	70.5	11.84

Table S4. Device parameters of PbS QDs solar cells with different numbers of photoactive layers and different rinsing solvents.

PbS-TBAI	V_{OC} (V)	J_{SC} (mA/cm^2)	FF (%)	PCE (%)
40 mg/mL× 5 layers (MeOH)	0.56	25.14	66.5	9.37
40 mg/mL× 5 layers (ACN)	0.60	25.47	68.9	10.53
80 mg/mL×3 layers (MeOH)	0.58	25.90	64.9	9.75
80 mg/mL×3 layers (ACN)	0.62	26.68	70.2	11.61
120 mg/mL × 2 layers (MeOH)	0.55	23.98	61.3	8.08
120 mg/mL × 2 layers (ACN)	0.59	26.24	67.1	10.39
200 mg/mL × 1 layer (MeOH)	0.24	14.75	32.5	1.15
200 mg/mL × 1 layer (ACN)	0.33	17.04	39.4	2.21

References

[S1] M. J. Speirs, D. M. Balazs, D. N. Dirin, M. V. Kovalenko, M. A. Loi, *Appl. Phys. Lett.* **2017**, *110*, 103904.

[S2] M. J. Speirs, D. N. Dirin, M. Abdu-Aguye, D. M. Balazs, M. V. Kovalenko, M. A. Loi, *Energy Environ. Sci.* **2016**, *9*, 2916-2924.